

Article

Unique Features of a New Baeyer–Villiger Monooxygenase from a Halophilic Archaeon

Mattia Nero ¹, Irene Righetto ¹, Elisa Beneventi ¹, Patrizia Polverino de Laureto ² ,
Marco Wilhelmus Fraaije ³ , Francesco Filippini ^{1,*} and Elisabetta Bergantino ^{1,*} 

¹ Synthetic Biology and Biotechnology Unit, Department of Biology, University of Padova, viale G. Colombo 3, 35121 Padova, Italy; mattia.niero87@gmail.com (M.N.); irene.righetto@bio.unipd.it (I.R.); elisa.beneventi@gmail.com (E.B.)

² Department of Pharmacological and Pharmaceutical Sciences, University of Padova, via F. Marzolo 5, 35131 Padova, Italy; patrizia.polverinodelaureto@unipd.it

³ Molecular Enzymology Group, University of Groningen, Nijenborg 4, 9747AG Groningen, The Netherlands; m.w.fraaije@rug.nl

* Correspondence: francesco.filippini@unipd.it (F.F.); elisabetta.bergantino@unipd.it (E.B.)

Received: 18 December 2019; Accepted: 14 January 2020; Published: 16 January 2020



Abstract: Type I Baeyer–Villiger monooxygenases (BVMOs) are flavin-dependent monooxygenases that catalyze the oxidation of ketones to esters or lactones, a reaction otherwise performed in chemical processes by employing hazardous and toxic peracids. Even though various BVMOs are extensively studied for their promising role in industrial biotechnology, there is still a demand for enzymes that are able to retain activity at high saline concentrations. To this aim, and based on comparative in silico analyses, we cloned *HtBVMO* from the extremely halophilic archaeon *Haloterrigena turkmenica* DSM 5511. When expressed in standard mesophilic cell factories, proteins adapted to hypersaline environments often behave similarly to intrinsically disordered polypeptides. Nevertheless, we managed to express *HtBVMO* in *Escherichia coli* and could purify it as active enzyme. The enzyme was characterized in terms of its salt-dependent activity and resistance to some water–organic-solvent mixtures. Although *HtBVMO* does not seem suitable for industrial applications, it provides a peculiar example of an alkalophilic and halophilic BVMO characterized by an extremely negative charge. Insights into the behavior and structural properties of such salt-requiring may contribute to more efficient strategies for engineering the tuned stability and solubility of existing BVMOs.

Keywords: Baeyer–Villiger monooxygenase; archaeon; recombinant halophilic enzyme; bioconversions; protein electrostatics; normal modes analysis

1. Introduction

The transformation of ketones to esters or lactones by peracids is known as Baeyer–Villiger oxidation. In synthetic organic chemistry, it represents a powerful methodology to insert an oxygen atom into a carbon–carbon bond. Although the reaction has a wide range of applications in the synthesis of fine chemicals [1], the standard protocol for Baeyer–Villiger oxidation encounters several drawbacks. For example, organic peracids are strong oxidants and display poor selectivity. Moreover, their use may lead to the formation of the corresponding carboxylic acid salt as waste, which has to be recycled or disposed of [2]. Furthermore, organic peracids are expensive and hazardous compounds. Among the alternative methods, which aim to bypass both the environmental and safety issues associated with the chemical approach, the use of Baeyer–Villiger monooxygenases (BVMOs) as biocatalysts for Baeyer–Villiger oxidations represents one of the most attractive approaches. BVMOs are flavoenzymes, which utilize molecular oxygen, instead of a peracid, as the stoichiometric oxidant and often exhibit a

broad substrate specificity while displaying high regio-, chemo-, and enantioselectivity [3]. In recent years, the identification of numerous novel BVMOs has led to a better understanding of the biocatalytic properties of these enzymes and to a continuous expansion of the enzymatic toolbox for their potential industrial application. Nevertheless, the present set of BVMOs is still far from meeting all industrial demands. Indeed, many available enzymes do not withstand industrial reaction conditions, which may involve the use of high temperatures, an acidic or alkaline environment or the presence of organic solvents. This prompted us to search for novel robust BVMOs in microorganisms able to thrive in extreme environments.

Extremophilic microorganisms represent an underutilized and innovative source of novel enzymes called extremozymes, able to catalyze chemical reactions whilst withstanding harsh conditions [4]. Only three robust BVMOs have been described so far: the phenylacetone monooxygenase (PAMO) from *Thermobifida fusca* [5]; a cyclohexanone monooxygenase (CHMO) from *Thermocrisium municipale* DSM 44,069 [6]; a polycyclic ketone monooxygenase from the fungus *Thermothelomyces thermophila* [7]. These three extremozymes were identified among the available genomes of (meso)thermophilic microbes. Although the most representative organisms of extreme environments belong to the Archaea domain, BVMOs do not seem to be widely distributed among these microorganisms. However, we could take advantage of the fully sequenced genome [8] of *Haloterrigena turkmenica* DSM 5511, an extreme halophilic organism originally isolated from a sulfate saline soil in Turkmenistan, in identifying *HtBVMO* as the first BVMO from an archaeon. A peculiarity of halophilic archaeobacteria (Haloarchaea) is that they counterbalance the external high salt concentration by the intracellular accumulation of inorganic ions. This is in contrast to halophilic eukaryotes and eubacteria, which overcame the extracellular osmotic pressure by accumulating organic molecules as osmoprotectants [9,10]. As a consequence, the soluble proteins and the intracellular components of haloarchaea are adapted to be functional at high intracellular salt concentrations [11,12]. Such an adaptation might be of biotechnological interest, due to the potential stability of macromolecules from haloarchaea in low water environments, such as various aqueous/organic media employed in biocatalytic reactions [13].

We report here that, in addition to being a halophilic enzyme, *HtBVMO* is also alkalophilic and shows the most electronegative surface among the BVMOs characterized so far. The expression and purification of polyextremophilic proteins such as *HtBVMO* can be challenging but can also result in important lessons, as understanding the structural features of a protein that is stable in one set of extreme conditions may provide clues about the activity of the protein in other extreme conditions [14]. We could successfully overexpress *HtBVMO* in a standard *E. coli* cell factory and carried out a detailed biochemical characterization. We investigated the effect of high pH and salt concentrations on the performance of this alkalo- and halophilic enzyme, explored its use in in vitro conversions and tested its tolerance to some water–organic-solvent mixtures. Noticeably, the proteome-wide in silico comparison of BVMOs by means of surface electrostatics and normal modes allowed the identification of predictive protocols to distinguish potentially soluble enzymes from insoluble ones, which may be of interest to the general biocatalysis community.

2. Results

2.1. Identification, Structural Modeling and Electrostatic Analysis of *HtBVMO*

The protein sequence of PAMO, a well-known BVMO from *T. fusca* (UniProtKb AC Q47PU39) was used as a tBLASTn query at the NCBI server. In order to exclude genes coding for flavoprotein monooxygenases that do not catalyze Baeyer–Villiger reactions, the search was further refined by looking for the presence of regular expression (pattern) FxGxxxHxxxWD/P, which is a unique sequence motif for Type I BVMOs [15]. Among the retrieved sequences, we looked for putative BVMOs, focusing on organisms that are unusual for this enzyme class, e.g., extremophiles. Following these criteria, we identified a putative BVMO from the extremely halophilic archaeon *Haloterrigena turkmenica*: *HtBVMO*. The genome of this organism was fully sequenced in 2010 [8] and comprises one main

circular chromosome and six circular plasmids. The gene encoding *HtBVMO* was identified in plasmid pHTUR01. *HtBVMO* shows 50% sequence identity with PAMO and conserved regions containing a number of known structural and functional motifs: (i) two Rossmann fold motifs (GxGxxG/A), involved in dinucleotide cofactor binding [16], (ii) the aforementioned motif for Type I BVMOs, (iii) the [A/G]GxWxxxx[F/Y]P[G/M]xxxD and (iv) Dx[I/L][V/I]xxTG[Y/F] motifs, all identifying this sequence as a putative BVMO [15,17,18]. A Clustal Omega alignment of *HtBVMO* with PAMO and CHMO from *Acinetobacter* NCIMB 9871 is shown in supplementary Figure S1. A feature that emerged from the sequence analysis is the low calculated pI of 4.19, due to a relatively high number of acidic residues (the total amount of aspartic and glutamic acid is roughly 20%). To investigate the distribution of charges, we generated a structural model of the protein using SWISS-MODEL [19], which proposed the structure of PAMO from *T. fusca* as the best template, in accordance with sequence homology data. Since the distribution of surface charges is influenced by the orientation of the side chains, the model was refined using SCWRL [20] and its final quality was evaluated via QMEAN server [21] (see methods); the calculated a Q-mean score of 0.757 assessed the model as very good among the alternative ones. The electrostatic potential for *HtBVMO* was estimated (see methods) and was compared with that of PAMO at increasing ionic strength. Figure 1 shows that *HtBVMO* is characterized by an extremely high negative potential, spread over the entire surface (depending on the presence of many Asp and Glu residues exposed to the solvent in the 3D model) and highlights an intriguing difference in the surface denegativization profiles of the two BVMOs.

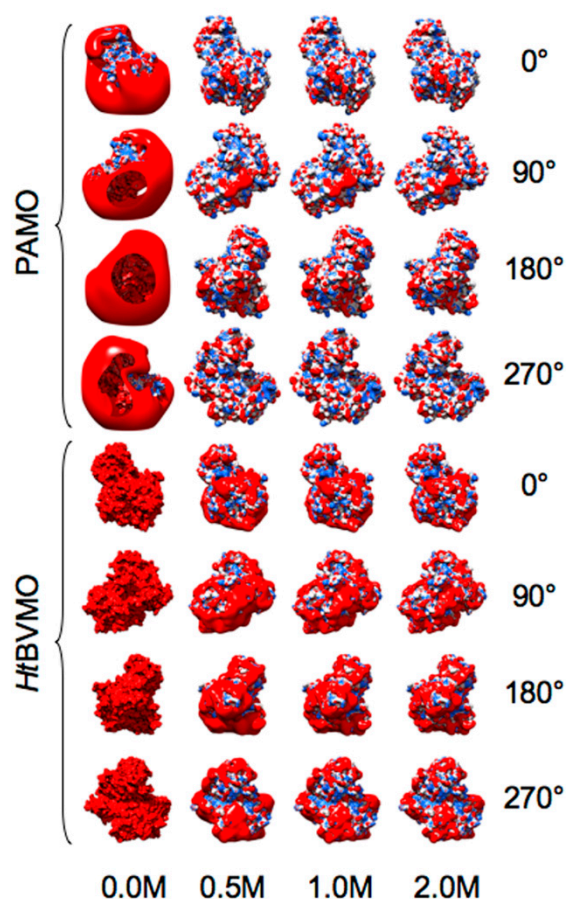


Figure 1. Comparison of the surface electrostatic isopotential contours of PAMO and *HtBVMO* at increasing NaCl concentrations. The electrostatic analysis was performed as reported in the Materials and Methods section, based on coordinates from the PAMO-solved structure (PDB 1W4X) and the *HtBVMO* structural model (PAMO is the template). Four views, 90° step angle of rotation are provided. Electrostatic potential is color-coded: red, negative; white, neutral; blue, positive.

The electrostatic isocontours of both proteins are highly negative (red color) in the absence of salt, even if a few neutral (white) or positive (blue) patches are evident in PAMO, while *HtBVMO* is fully negative and the isocontour “cloud” is so large that it cannot be viewed in the observation box. When salt concentration is brought up to 0.5 M, denegativization of the PAMO surface is clearly evident and further increases in salt concentration do not result in a meaningful change in the PAMO electrostatic isocontour at 1.0 or 2.0 M concentrations. Instead, the denegativization of *HtBVMO* along increasing concentration is lower than PAMO and progressive, clearly suggesting that this enzyme, in addition to being putatively halophilic, is alkalophilic as well. An enrichment in negative charges at the protein surface had already been observed in the crystal structure of other halophilic proteins (e.g., glucose dehydrogenase from *Haloferax mediterranei* [22], malate dehydrogenase [23] and ferredoxin from *Haloarcula marismortui* [24]) and is supposed to favor solvation. This feature, together with a reduction in basic amino acids (particularly lysines) and a decrease in the overall hydrophobic content, are characteristic signatures of the hypersaline adaptation of proteins [25–27].

2.2. Comparative Electrostatic and Normal Modes Analysis of *HtBVMO*

Table 1 compares the amino acid surface accessibility of *HtBVMO* to those generated for the thermophile PAMO (PDB: 1W4X), the mesophile *RhCHMO* (from *Rhodococcus* sp., PDB: 3GWD), and the well-characterized halophile enzyme *HmMDH* (PDB: 4JCO), a malate dehydrogenase from *Haloarcula marismortui*. It is worth noting that, although the overall ratio between the charged and hydrophobic residues is comparable in all the proteins (ranging from 0.5 to 0.61), the ratio of acidic over basic residues is twofold higher in the two halophilic enzymes. However, when only surface residues are considered, *HtBVMO* shows the highest ratio between the exposed charged and hydrophobic residues.

Table 1. Comparison of amino acid surface accessibility.

	<i>HtBVMO</i>	<i>Halophilic</i> <i>HmMDH</i>	<i>Thermophilic</i> PAMO	<i>Mesophilic</i> <i>RhCHMO</i>
Amino acid frequencies (% of total residues)				
Asp+Glu	21.66	20.39	13.84	14.44
Arg+Lys	7.84	7.57	10.30	8.89
Hydrophobic residues	41.70	49.67	47.20	51.85
Amino acid ratios				
(Asp+Glu)/(Arg+Lys)	2.73	2.70	1.34	1.63
Charged/hydrophobic	0.52	0.61	0.51	0.50
Accessible surface (Å²)				
Total	22,733.40	13,352.55	22,158.52	21,277.37
Asp+Glu	9648.94	4880.15	5403.37	6154.71
Arg+Lys	3040.31	1744.19	5143.93	4379.64
Hydrophobic residues	4536.05	3407.03	6413.00	6134.00
Amino acid surface ratios				
(Asp+Glu)/(Arg+Lys) surface ratio	2.88	2.80	1.05	1.41
Charged/hydrophobic surface ratio	2.73	1.94	1.64	1.41
% of total surface				
Asp+Glu	42.44	36.55	24.39	28.93
Arg+Lys	14.72	13.06	23.21	20.58
Hydrophobic residues	19.95	25.52	28.94	28.83

Notably, 42% of the total accessible surface of *HtBVMO* consists of acidic residues; the relatively high overall negative charge is also explained by a significant reduction in positively charged (Lys and Arg) residues. On the whole, both the amino acid composition and the structural model show typical features of an extreme halophilic protein [25,26]. However, the highly negative surface of *HtBVMO* prompted us to further investigate this feature in comparison to other known halophilic and non-halophilic BVMOs. These enzymes have been classified into seven groups (plus a further group

of non-classified outliers) based on phylogenetic clustering [28]. We considered the fifty BVMOs from this article, representative of the seven classes, added *Ht*BVMO and ranked all of them on the basis of protein net charge (see supplementary Table S1). An intriguing evidence inferred from this analysis is the large variation in net charge within each class, with BVMOs from all classes but five being negatively charged. Positively charged BVMOs (+1 to +7) are present only in Class 5, where the most negative enzyme has -9 net charge. The negative charge in Classes 2, 3, 4, 6 and 7 ranges from close to neutral (e.g., -3) to values for the most negative representative enzymes, such as -16 (Class 6), -23 (Class 4) and -31 (Classes 2, 3 and 7). A similar range would also characterize Class 1 (net charge from -4 to -28) when not considering *Ht*BVMO, which has a -73 net charge instead and remains a “special” BVMO (with forty-two extra negative charges with respect to the second most negative BVMO) even when extending the comparison to Table S1, i.e., to BVMOs in the databases (data not shown).

The evidence that phylogenetic-based grouping into the seven reported classes [28] is not in agreement with net charge distribution (as it varies in each class, with highly overlapping ranges), prompted us to perform an electrostatics-based, comparative analysis of a set of 86 BVMOs (including *Ht*BVMO and other important enzymes not previously reported [28]). To this aim, we considered the distribution of the electric isopotential at the protein surfaces, which proved useful to identify putative fingerprints in a “functional” grouping and classification of proteins [29,30]. Since the atomic coordinates of three-dimensional structures, rather than simple sequences, are needed to perform such surface electrostatic analysis, and only six solved structures were available, 80 structural models were obtained via homology modelling, refined, and their quality assessed (see methods section for details on the software used, and the settings and steps, and supplementary Table S2 for enzyme names, Uniprot AC, and the modelling template for each protein in this complement). In order to perform analyses, taking into account the influence of ionic strength (I), the spatial distribution of the electrostatic potential was calculated at $I = 150$ mM (which is physiological for expression in a standard cell factory, such as *E. coli*), assuming $+1/-1$ charges for the counter-ions. Prior to electrostatic potential calculations, the overall set of Protein Data Bank (PDB) files were converted, replacing temperature and occupancy columns with columns containing the per-atom charge Q and radius R (PQR) to assign partial charges and van der Waals radii; then, linear Poisson–Boltzmann (PB) equation calculations were carried out by using Adaptive PB Solver (APBS) through Opal web service (see Methods). In order to evaluate electrostatic distance (ED) in a quantitative way, clustering of the spatial distributions of the electrostatic potentials was obtained, having the use of the Hodgkin and Carbo similarity index (SI) (see Methods for details and references). The Carbo SI is sensitive to the shape of the potential being considered but not the magnitude, whereas the Hodgkin SI is sensitive to both shape and magnitude. Therefore, results obtained using the Hodgkin SI are presented in this work, while analyses with the Carbo SI are not shown even if they were performed as well, confirming parameter independent data. “Heatmap” in Figure 2 shows the ED among the different BVMOs.

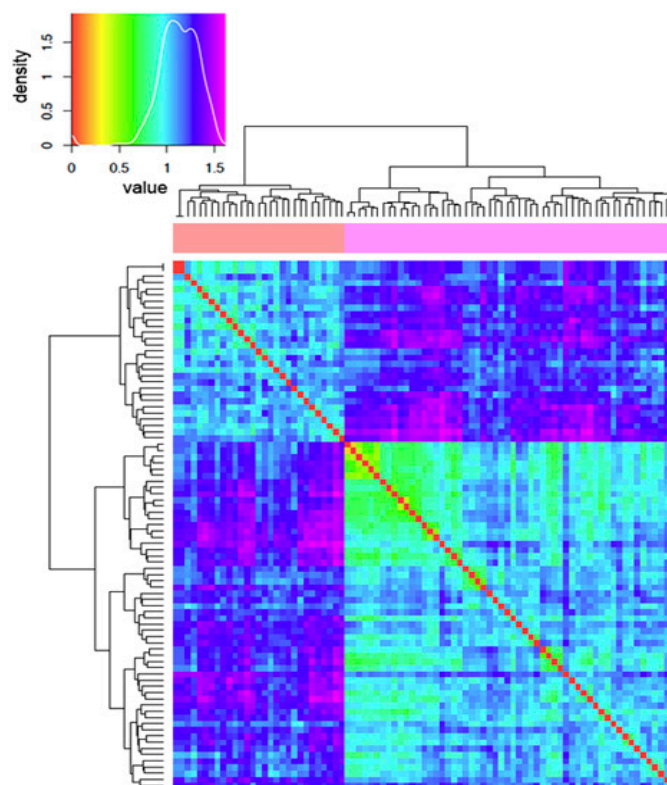


Figure 2. Clustering of Baeyer–Villiger monoxygenases (BVMOs) according to their electrostatic potential.

The color coding for the electrostatic distance (ED) is presented in the density plot (upper, small image); the lower image presents a reduced version (without individual accession numbers) of the heatmap. The complete, original heatmap is presented in supplementary Figure S2. Proteins are clustered according to their electrostatic potential using a color code from warm colors (small distance) to cold ones (large distance). The BVMOs taken into account are clearly grouped into two large supergroups (highlighted by salmon pink and magenta colors in the horizontal bar below the dendrogram); within each group the enzymes are electrostatically closer to each other (prevalence of cyan background), while high inter-group ED is apparent (as stated by dark cold colors).

When the associated epogram was inspected for BVMOs' sorting between the two supergroups (an epogram is similar, in data clustering representation, to a standard phylogenetic tree, even though it is based on ED instead; see supplementary Figure S3), it showed more evidently intriguing evidence. Indeed, the insoluble BVMOs are grouped in the smaller group, together with the whole Class 5 BVMOs, while *Ht*BVMO clustered together with potentially soluble BVMOs.

2.3. Normal Modes Analysis of *Ht*BVMO and Soluble/Insoluble Enzymes

In addition to electrostatics, we also took into account protein dynamics by performing Normal Modes Analysis (NMA) [31]. NMA allowed us to highlight further fingerprints for soluble vs. insoluble BVMOs. BVMOs from Class 1 (including *Ht*BVMO) and Class 5 were analyzed because of the presence of soluble and insoluble BVMOs in the same class. The insoluble enzyme in Class 1 is *Ht*BVMO1 from *R. jostii*RHA (Q0S1Y4), and two insoluble BVMOs belong to Class 5: *Af*BVMO2 from *A. fumigatus*Af293 (Q4WBK1) and *Rj*BVMO13 from *R. jostii*RHA (Q0SA63). However, only NMA for Class 1 BVMOs is presented here (Figure 3), where the insoluble enzyme *Rj*BVMO1 is highlighted in apple green in the fluctuation plot.

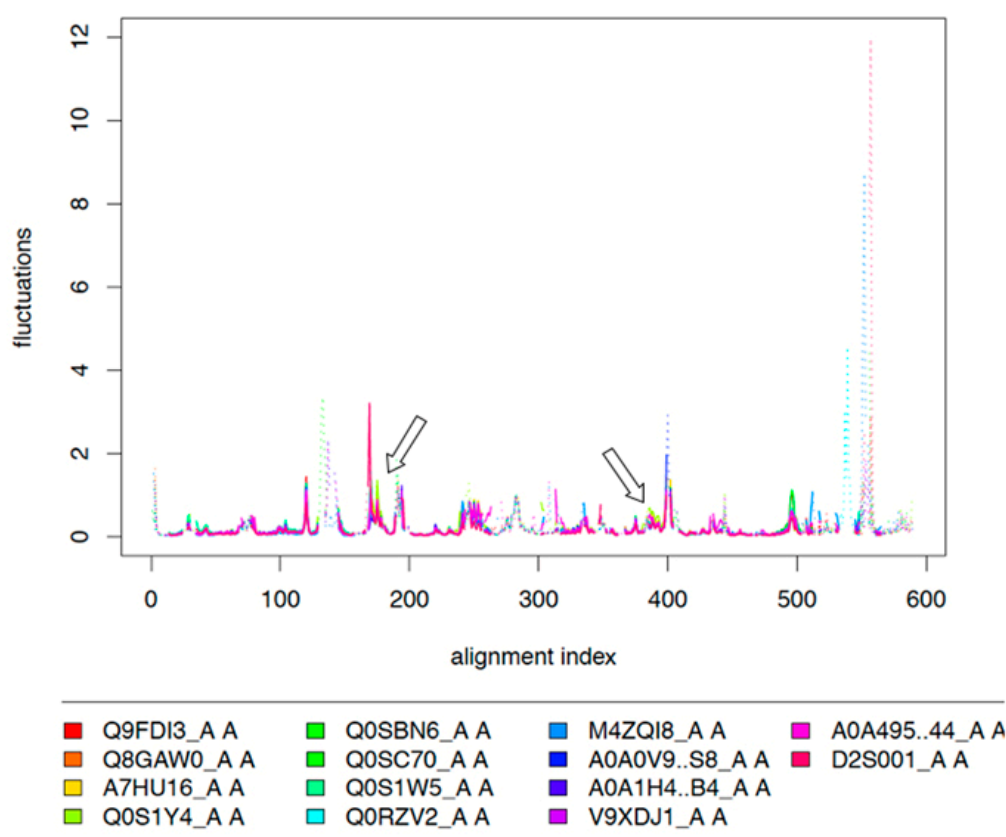


Figure 3. Comparative normalised fluctuation plot of the Class 1 BVMOs. The fluctuations describe the flexibility of the C α atoms of the enzymes. Residue numbers are given on the x-axis and the amplitude of fluctuations on the y-axis. The parts aligned with gaps in other structures are shown as dotted lines. Only *RjBVMO1* presents a spike around positions 180 and 390 (see arrows).

Similar peculiar results were obtained from the inspection of the Class 5 fluctuation plot, with spikes specific to the insoluble enzymes; however, the average % of identity to template structures of the Class 5 model structures (under 25%, with some negative quality assessment reports from QMEAN) suggests that further work is needed to distinguish the meaningful differences from some noise, and thus this plot is not shown. We also considered the Bhattacharyya coefficient (BC), which measures the dynamical similarity between proteins by comparing their covariance matrices, obtained from the normal modes of the conserved parts of the considered proteins [32]. However, even if the BC analysis confirmed intriguing data for Class 1 enzymes (e.g., the clustering of *HtBVMO* with soluble enzymes, with the insoluble *RjBVMO* showing a lower BC value), the BC maps are presented in the supplement (see Figure S4) for completeness of information, but they are not discussed in detail because of the aforementioned presence of lower quality models likely to result in disturbing noise.

2.4. Cloning, Expression, and Purification of *HtBVMO*

The genomic DNA of *H. turkmenica* was not considered as a starting material for PCR amplification of the gene of interest, since culture collections distributing the archaeon did not ensure the presence of plasmid pHTUR01 in their stocked strains. We, therefore, opted to use a synthetic gene that could be designed with optimized *E. coli* codon usage. In fact, sequence analysis revealed that 16% of the sense triplets in the native *HtBVMO* gene corresponded to rare codons in *E. coli*. The synthetic gene was cloned into the pET28a(+) expression vector for the expression of a His-tagged protein. Overexpression assays at different temperatures were performed using *E. coli* BL21(DE3). The recombinant protein was expressed as a soluble protein when cells were grown, and induction was carried out at 12 °C. After

IMAC chromatography, 8 mg of protein were obtained from one liter of culture. However, the purified protein was colorless, indicating that it did not contain the FAD cofactor, which is typically tightly bound to type I BVMOs and changes them to a yellow color. The activity of the recovered recombinant protein was tested by monitoring NADPH consumption in the presence of several ketone compounds as substrates, such as butan-2-one, nonan-3-one, and cyclohexanone. Yet, as expected, the purified protein did not display any activity. The lack of color and activity suggested that the protein was misfolded. This may be explained by considering that the source organism of the enzyme is described as requiring at least 2 M NaCl for growth. The strategy most frequently used by haloarchaea to cope with osmotic pressure involves the accumulation of high concentrations of ions, such as potassium and chloride; their soluble enzymes are, therefore, themselves adapted to a high salt environment [33]. Therefore, we modified the purification protocol by adding NaCl up to a concentration of 2 M, and the FAD cofactor to a final concentration of 100 μ M, to the lysate. Through this, we aimed to assure the ionic strength required for the folding of the protein, and permit an easy uptake of the cofactor during the process. Since protein folding requires some time, we incubated the cell lysate at 4 °C for at least 12 h. After the incubation, we recovered the soluble proteins and proceeded with nickel affinity chromatography and hydrophobic chromatography, always maintaining 2 M NaCl in the equilibration and elution buffer. Using this protocol, we were able to recover a recombinant form of *HtBVMO* (about 4 mg per liter of culture) that was bright yellow and active on nonan-3-one (see the following). It is worth noting that the protein displayed an aberrant electrophoretic mobility during SDS-PAGE (supplementary Figure S5). The apparent molecular weight was about 80 kDa, versus a calculated value of 63 kDa. To exclude unexpected modifications to the polypeptide, a peptide mass fingerprinting analysis of the protein in the acrylamide gel band was performed. This analysis confirmed the identity of the protein as the *HtBVMO*. Altered electrophoretic mobility is characteristic of proteins from halophilic organisms and is ascribable to the unusually high proportion of negatively charged residues, a typical trait of these proteins [34]. This feature reduces the binding of SDS molecules to the unfolded protein, thereby diminishing the mobility the SDS–protein complex. Such an alteration in electrophoretic behavior was also reported for other proteins purified from haloarchaea [35,36].

2.5. Salt and pH-Dependent Activity of the Recombinant Enzyme

Attempts to purify the recombinant *HtBVMO* in the absence of salt led to an inactive form of the protein. Therefore, the effect of salt concentration on the enzyme activity was studied using buffers containing 0–5 M NaCl or 0–4 M KCl, respectively (Figure 4a). With both salts, activity was clearly dependent on concentration: as previously stated, no activity was detectable in the absence of salt and the optimum was reached at 2.0 M NaCl or 3.0 M KCl.

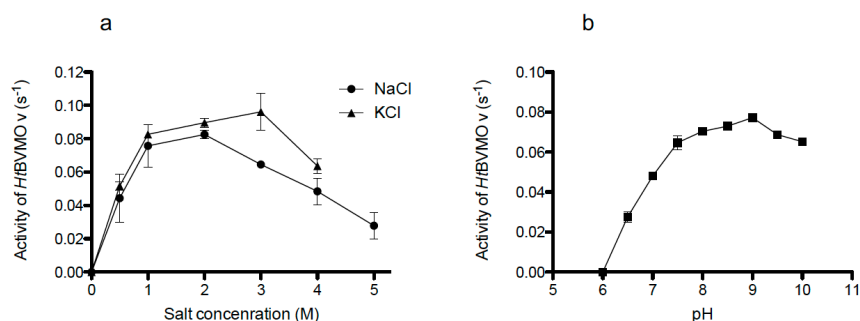


Figure 4. Effect of salt concentration and pH on the activity of *HtBVMO*. (a) Activity at constant pH (50 mM TRIS-HCl pH 8.0) and varying NaCl or KCl concentrations. (b) Activity at a constant salt concentration (2.0 M NaCl) and varying pH (TRIS-MES and acetate buffer). Values are means \pm SD (n = 3).

In order to check whether activity loss in the absence of salt would depend on the unfolding and/or denaturation, the active form of the protein was dialyzed for salt removal. As expected, no residual activity was detected after this step, even if 2.0 M NaCl was added in the enzymatic assay. Moreover, to explore the possibility of restoring enzyme activity, the inactive protein was dialyzed against different buffer solutions containing 0.5, 1.0, or 2.0 M NaCl. The FAD cofactor was also added to the dialysis solution to a final concentration of 100 μM , to warrant its inclusion in the protein during the refolding process. None of the tested conditions could restore activity. Based on the absolute requirement of high ionic strength for the enzymatic activity, we also monitored the NADPH consumption at different pH values, while maintaining a constant 2.0 M NaCl concentration (Figure 4b). For this assay, a buffer composed of TRIS, MES, and acetate was used, which covers a wide range pH spectrum (pH 5.5–10.0) [37]. The enzyme retained most of its activity at a pH between 7.5 and 10.0, reaching the optimum at pH 9.0. Below pH 7.5, the activity rapidly decreased, reaching 35% at pH 6.5, while no activity was exhibited at pH 6.0. Considering the amino acid composition and the peculiar electrostatic features of *HtBVMO*, the protein is likely to require a basic pH to preserve the negative charges of its acidic residues, which may have a role in maintaining the active form of the protein.

2.6. Salt-Dependent Folding of *HtBVMO*

To assess whether the salt-dependent activity of the recombinant enzyme was related to the degree of folding, we recorded the far- and near-UV circular dichroism (CD) spectra of the enzyme in the presence of different NaCl concentrations. The CD spectrum in the far-UV region (190–250 nm) can be used to provide quantitative estimates of the secondary structure content in a protein. We therefore monitored the conformational changes brought about on *HtBVMO* by variations in the surrounding ionic strength. CD data were collected from 202 nm and 250 nm, avoiding light absorption and the noise contribution of chloride ions in the 190–200 nm region. Although fluoride salts such as KF or NaF would be preferred (fluoride ion does not adsorb light in the far-UV region), NaCl was chosen to allow a comparison with already collected biochemical and kinetic data. As shown in Figure 5a, the registered far UV-CD spectrum of *HtBVMO* in the presence of 0.1 M NaCl was typical for an unfolded protein, as indicated by the negative ellipticity at 200 nm and by the modestly negative ellipticity in the 210–225 nm region.

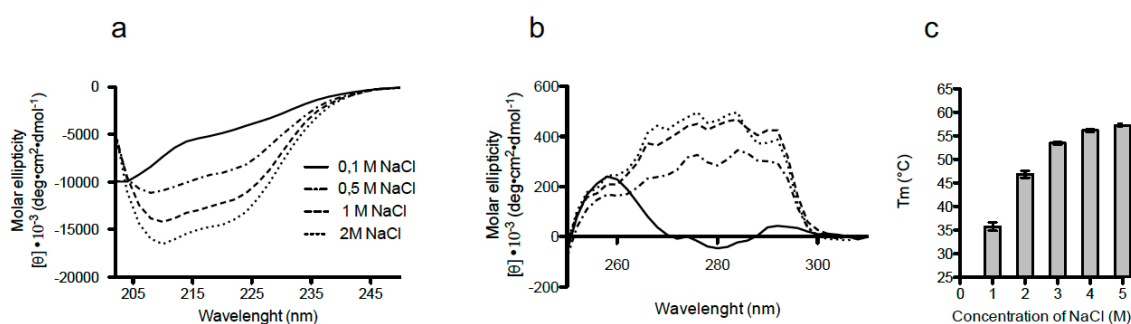


Figure 5. Salt-dependent folding of *HtBVMO*. (a) Far-UV and (b) Near-UV Circular Dichroism spectra of 0.1 mg/mL enzyme in 50 mM TRIS-HCl buffer pH 8.0 in the presence of increasing concentrations of NaCl (0.1–2.0 M). (c) Thermal stability of *HtBVMO* measured in solutions at increasing molarity of NaCl.

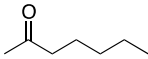
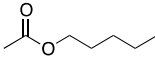
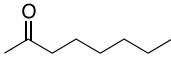
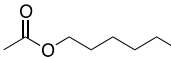
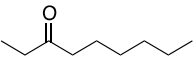
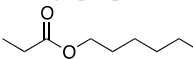
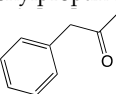
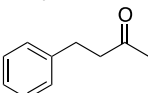
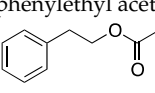
Increasing the salt concentration led to a more pronounced negative ellipticity, implying a progressive acquisition of overall α -helical content. Based upon the deconvolution of the CD spectra, the α -helical content was found to decrease from 35% to 23% when lowering NaCl concentration from 2.0 to 0.5 M. The conformational changes of *HtBVMO* exposed to different ionic strengths were further studied by monitoring the CD spectra in the near-UV region (250–310 nm). The CD profile in this wavelength region primarily arises from the environments of each aromatic amino acid side

chain [38]. In the case of the folded *HtBVMO* (2.0 M NaCl), the side chains of these amino acids are supposed to be placed in a variety of asymmetric environments characteristic of the tertiary structure of the folded protein. Figure 5b shows a decreasing intensity of the CD spectra profiles consistent with the decrease in salt concentration. The lower ionic strength may increase the flexibility of the protein and contribute to higher mobility of the aromatic side chain, influencing the CD signals. These results indicated that a high salt concentration is a strict requirement for the maintenance of protein folding and, as a consequence, its activity. This conclusion was further confirmed by analyzing the thermostability profile of the protein. The melting temperatures (T_m) of the protein at different salt concentrations were measured by a fluorescence-based thermal stability assay. As shown in Figure 5c, the T_m increases from 35.7 °C at 1 M NaCl to 57.3 °C at 5 M NaCl. The increasing thermal stability between 2 and 5 M NaCl does not correlate with enhanced activity of the enzyme. In fact, although the highest melting temperature was found at a salt concentration near the saturation level, the protein is not fully active in this environment. This is probably due to the structural rigidity reached at an extreme ionic strength, which constrains the conformational mobility required for catalysis.

2.7. Steady-State Kinetics

In order to explore the substrate preference of *HtBVMO*, a set of ketones that are often-accepted substrates for BVMOs were tested. Linear aliphatic ketones, cyclic aliphatic ketones and aromatic ketones were selected as substrates and tested in the same reaction conditions: 25 °C, 50 mM TRIS-HCl, pH 8.0, 2.0 M NaCl and 100 μ M NADPH. By measuring enzyme activities at different ketone concentrations, the steady-state kinetic parameters for the accepted substrates were obtained (Table 2).

Table 2. Steady-state kinetic analysis of *HtBVMO*.

Substrate	K_M (mM)	k_{cat} (s^{-1})	k_{cat}/K_M ($s^{-1} \text{ mM}^{-1}$)	Product
heptan-2-one 	0.09 ± 0.01	0.277 ± 0.005	3.08 ± 0.35	pentyl acetate 
octan-2-one 	0.7 ± 0.1	0.27 ± 0.02	0.38 ± 0.06	hexyl acetate 
nonan-3-one 	4.5 ± 1.3	0.12 ± 0.01	0.260 ± 0.008	hexyl propionate 
1-phenylpropan-2-one 	no reaction	no reaction	no reaction	no product
4-phenylbutan-2-one 	0.017 ± 0.002	0.155 ± 0.003	8.90 ± 0.89	2-phenylethyl acetate 

Enzymatic assays for kinetic parameters determination were carried out under the same reaction condition: temperature of 25 °C, 50 mM TRIS-HCl, pH 8.0, 2 M NaCl and 100 μ M NADPH. The conversions of substrates into products were performed in a 1.0 M NaCl buffer in order to couple *HtBVMO* and *PsPTDH* activities.

In general, the enzyme showed a preference for aliphatic linear ketones. The k_{cat} values for the identified substrates were all quite similar (around 0.2 s^{-1}), with the highest values registered for octan-2-one and heptan-2-one. More significant differences were observed in K_M values. Among the aliphatic ketones, heptan-2-one was found to be the preferred substrate, with a K_M of 0.09 mM and a k_{cat} of 0.277 s^{-1} . Cyclic ketones, such as cyclopentanone, cyclohexanone, 4-methyl-cyclohexanone and aromatic ones, such as indan-1-one, acetophenone and phenylacetone, were not accepted as

substrates. Interestingly, the enzyme showed the highest affinity ($K_M = 0.017$ mM) and catalytic efficiency ($k_{cat}/K_M = 8.90$ s⁻¹ mM⁻¹) for 4-phenylbutan-2-one, despite its somewhat low k_{cat} value (0.15 s⁻¹). This suggests that the longer carbon chain substituent on the aromatic ring could be a discriminant factor for the acceptance of the compound as a substrate.

2.8. Enzymatic Conversions

We also tested *HtBVMO* for the in vitro conversion of substrates into ester products, by using phosphite dehydrogenase from *Pseudomonas stutzeri* (*PsPTDH*) [39] as a cofactor regeneration enzyme. The effects of NaCl, MgSO₄, and MgCl₂ in a range of 0.1–1.0 M were studied on the activity of both *PsPTDH* and *HtBVMO*, with the aim of finding the proper reaction conditions for both enzymes (Figure 6). For all tested salts, concentrations higher than 0.2 M resulted in relatively low *PsPYDH* activity.

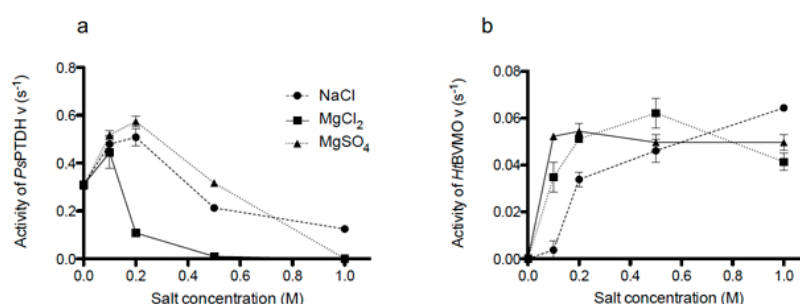


Figure 6. Activity of *PsPTDH*. (a) and *HtBVMO* (b) in the presence of 0–1.0 M NaCl, MgSO₄ and MgCl₂.

For the latter enzyme, at the highest concentration of 1.0 M, NaCl was the only tolerated salt, with a residual activity of 40%. The stability of both *PsPTDH* and *HtBVMO* in 1.0 M NaCl was evaluated by monitoring their activity for 5.5 h (time 0; then after 1, 2.5 and 5.5 h). In this time window, both the enzymes remained almost fully active. Therefore, 1.0 M NaCl was chosen as the condition for testing the biotransformations of some ketones by GC-MS analysis. All accepted substrates in Table 2 were completely converted by *HtBVMO* to the ester products, with a conversion of at least 99%. As a further observation, enzymatic assays carried out in magnesium sulfate/chloride demonstrated that the activity of *HtBVMO* depends not only on concentration but also on the nature of the salt (Figure 6b). This behavior was already reported for halophilic malate dehydrogenase and suggested a more efficient interaction of highly charged cations and anions with the folded form of halophilic proteins [40].

Besides the in vitro conversions, we set out to examine the activity of the enzyme in the whole-cell configuration. This experiment was conceived to further inquire about the presence of somewhat active forms of the enzyme in the cytosol of recombinant *E. coli* cells. Heptan-2-one and nonan-3-one were chosen as substrates. The biotransformations were performed using resting cells: BL21 *E. coli* cells expressing the enzyme *HtBVMO* or *CmBVMO* (from the eukaryote unicellular red alga *Cyanidioschyzon merolae* [41]), the latter used as a control for the test, were grown and induced in the same conditions used to purify the halophilic enzyme. Recombinant bacteria were then harvested and resuspended in a phosphate buffer supplemented with glucose and the substrate, and further incubated at 20 °C for 48 h. The GC analysis (supplementary Figure S6) of the control samples showed the partial conversion of heptan-2-one and nonan-3-one to pentyl acetate and hexyl propionate, respectively, as expected. No ester products could be observed in reactions performed by bacteria expressing the *HtBVMO*, suggesting that the archaeal enzyme produced in the cytosol of *E. coli* is not fully competent for activity.

2.9. Activity of *HtBVMO* in Aqueous–Organic Media

The effect of different water-miscible organic solvents on the activity of *HtBVMO* was investigated. Residual activity, with respect to that observed in the absence of solvent in 3.0 M KCl, showed that dioxane and methanol are tolerated by the enzyme (Figure 7).

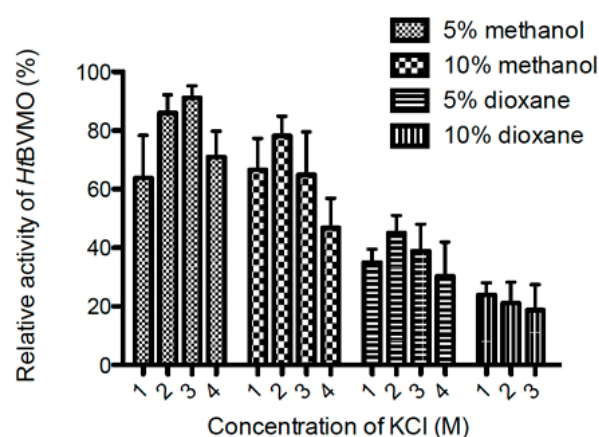


Figure 7. Organic solvents' effect on the activity of *HtBVMO* at different concentrations of KCl (M). Enzyme activity was assayed under standard conditions; results were expressed as relative activities (%) with respect to that observed in the absence of solvent at 3 M KCl.

Interestingly, it was found that the cosolvents had an effect on the salt requirements of the enzyme. In the presence of 5% (*v/v*) methanol, the enzyme showed its best activity at 3.0 M KCl, while in the presence of 5% dioxane the optimum salt concentration was reduced to 2.0 M KCl. In both cases, doubling the solvent ratio changed the salt preference toward lower concentrations: 2.0 M KCl in 10% methanol and 1.0 M KCl in 10% dioxane. Methanol was found to be a better co-solvent than dioxane, as the enzyme maintained 90% of its activity in the presence of methanol, while lower activities were observed when dioxane was used. Higher solvent concentrations were tested but technical difficulties, such as salt precipitation, prevented proper measurements.

3. Discussion

We report here on the characterization of the first Baeyer–Villiger monooxygenase discovered in the Archaea domain. This enzyme, from *Haloterrigena turkmenica*, is also the first BVMO showing typical features of halophilic proteins: salt-dependent activity and denaturation at low salt concentrations. In addition, it shows a very high number of negatively charged amino acids in its primary sequence, resulting in a net charge of -73 that is unique among known BVMOs and suggests this enzyme to be both halophilic and alkaliphilic. Up to now, halophilic adaptation has been best explained by the solvation stabilization model, deduced from the biochemical and crystallographic data obtained for the malate dehydrogenase of *Haloarcula marismortui* (*HmMDH*) [42], as well as from the results of extensive mutagenesis experiments conceived to assign or to rescue the halophilic character to selected proteins [26]. The key factor of this model is the reduction in the accessibility of the solvent to the surface of the protein in an environment where water molecules are mainly engaged in ion solvation. This is achieved by increasing the number of acidic residues, as well as aspartate and glutamate. Indeed, even though carboxyl groups of acidic amino acids are also strongly hydrated in an unfolded polypeptide, they only contribute to the stability of the halophilic protein in high-salt environments when they are precisely arranged on the protein surface; the electrostatic isocontour analysis confirms that *HtBVMO* is endowed with an exceptionally negative surface. This reduces the tendency of the protein to aggregate and increase its solubility at physiological pH by lowering the isoelectric point. A reduction in the number of lysines and arginines at the surface also increases the halophilicity, independently of the charge, since their long side chains would favor the accession of the solvent to the exposed amine groups. Conversely, these features also cause protein destabilization in the absence of salt and result in the misfolding of halophilic proteins in low-salt conditions—that is, in physiological aqueous solutions such as the cytoplasm of non-halophiles.

The halophilic character and behavior of *HtBVMO* have been verified at both the theoretical level (surface charge distribution in the 3D protein model) and the biochemical one (denaturation of the

protein and loss of activity occurring at low salt concentrations). Moreover, comparative electrostatics and NMA helped to predict that *HtBVMO* shares surface and motion fingerprints with “soluble” BVMOs, while unveiling intriguing evidence about the clustering of non-soluble ones. Despite such features, we managed to develop the production as well as the purification of the folded and active form of the protein. The designed purification protocol leads to speculation about the presence of ‘on-pathway’, partially folded forms of *HtBVMO* (as opposed to ‘off-pathway’, irreversibly unfolded ones) inside the *E. coli* cytosol. Such forms would be the result of a very low speed of translation and folding, obtained by growing the cells at 12 °C after induction, a key step in the obtainment of an active enzyme. In vivo, during and after protein synthesis, the partially folded forms of the protein might be stabilized by the overall charges of macromolecules and metabolites of the crowded matrix of the cytosol (where the physiological NaCl concentrations are about 4 mM; [43]). The results of whole-cell experiments seem to support this speculation: in the cytosol of *E. coli*, the synthesized *HtBVMO* appeared inactive, differently from the homologous mesophilic *CmBVMO* (43% amino acid identity, 63% similarity) that was shown to be already competent for catalysis. Nevertheless, the presence of the FAD cofactor together with NaCl at high concentrations at the moment of cell disruption seemed to allow further completion of folding (over at least 12 h at a very low temperature, 4 °C), as well as the acquisition of activity and stabilization of the final enzyme.

We were able to carry out the conversions of distinct ketones by coupling the Baeyer–Villiger oxidation with a regeneration reaction catalyzed by a phosphite dehydrogenase (PTDH), at a concentration of NaCl which allows the activity of both enzymes. Although the final reaction condition was a necessary compromise and not the ideal one for either enzyme, the conversions were efficiently catalyzed. A possible alternative to PTDH could be the glucose dehydrogenase from the haloarchaeon *Haloferax mediterranei* [44], although its use in bioconversion as a cofactor regeneration enzyme in combination with a halophilic catalyst has not been reported in the literature. To the best of our knowledge, the one that we describe here is the first example of a bioconversion carried out with a halophilic enzyme that requires a cofactor regeneration system.

The applicability of this peculiar BVMO was also examined in relation to its activity and stability in the presence of the two organic solvents: methanol and dioxane. Catalysis in organic media offers several advantages: for example, a minor tendency of both substrates and products to be hydrolyzed, the elimination of microbial contaminations in the reaction media and, above all, the higher solubility of hydrophobic substrates [13]. Enzymes from non-halophilic organisms often do not tolerate organic solvents [45]. Conversely, halophilic enzymes work in extremely high salt concentrations, and considering that salt tends to greatly reduce water activity, these enzymes may also perform well in other low water activity environments, such as organic solvents or aqueous/organic mixtures [13]. Various halophilic enzymes have been reported to be active and stable in the presence of different organic solvents, e.g., proteases [46,47], dehydrogenases [48,49] and amylases [50,51].

Considering its strict dependency on a high salt content, the applicability of *HtBVMO* in synthetic chemical processes might be considered of limited potential help, due to inherent operational difficulties (in the regeneration of the oxidized nicotinamide cofactor and preventing the corrosion of industrial equipment). However, the newly discovered halophilic BVMO might furnish some further clues to study the resistance towards organic solvents of this class of enzymes. Indeed, this lack of stability is the Achille’s heel that has, to date, hampered their exploitation in industrial processes and has prompted various engineering attempts to improve their properties [52–54]. Their improvement, in terms of tolerance to organic solvents, as well as to high temperatures and oxidative stress, still needs to be improved as a requisite for applicability. In addition to being a halophilic enzyme, *HtBVMO* is alkalophilic as well, as predicted by its special net charge, electrostatic features and confirmed by its alkaline optimal pH. This makes *HtBVMO* a representative polyextremophilic enzyme, whose characterization may provide important lessons both in basic investigations about the adaptation to extreme conditions and in setting up biocatalysts able to be effective under harsh conditions.

4. Materials and Methods

4.1. Bioinformatic Identification, Structural Modeling and Electrostatics Analysis

Gene identification and alignments were performed using BLAST and Clustal Omega algorithms, respectively [55]. *E. coli* codon usage analyzer 2.1 was used for rare codon analysis and sequence optimization [56]; theoretical parameters of the protein were calculated using the ExPASy ProtParam tool [57]. A structural model of *HtBVMO* was generated by homology modeling, using the Swiss-Model Server [58] and the crystal structure of PAMO (PDB code: 1W4X) as a template. The model structure was refined using SCWRL [20] and the quality of the final model was checked via the QMEAN server [21]. Solved or modeled structures were viewed using UCSF Chimera [59] v. 1.14 (free download from [60]). For the analysis of *HtBVMO* and PAMO surface electrostatic potentials, PDB2PQR [61] was used to assign partial charges and van der Waals radii according to the PARSE force field [62]. Linear Poisson–Boltzmann equation calculations were then carried out by using the Adaptive PB Solver [63] through the Opal web service [64]. The calculation was done using protein and solvent dielectric constants of 2 and 78.5, respectively [65,66], with $T = 298.15$ K and ionic strength equal to 0, 0.5, 1.0 or 2.0 M. Rigid-body superposition was performed, and electrostatic potential was computed using Chimera 1.14. Electrostatic distance (ED) [67] was calculated using the Hodgkin index and the Carbo index at the WebPIPSA server [68]. Amino acid surface accessibilities were calculated by the online software GetArea [69], setting a water probe radius of 1.4 Å.

4.2. Single and Comparative Normal Mode Analysis

Single and comparative NMA analyses were performed using the WebNM@ server [32]. This tool is able to calculate the low-frequency normal modes by building the coarse-grained Elastic Network Model (ENM) of a submitted pdb file [31], returning the protein, represented as a string of beads of C_{α} atoms. In this work, the default settings of WebNM@ were used. PDBeFOLD [70] was used to perform structural alignments, requested by the WebNM@ server. This kind of analysis is useful to investigate the dynamic similarity in terms of the Bhattacharyya coefficient (BC) and Root Mean Square Inner Product (RMSIP) [32]. The BC measures the dynamical similarity between proteins by comparing their covariance matrices, obtained from the normal modes of the conserved parts of the considered proteins. BC values range from 0 to 1. A BC of 1 represents the maximum overlap (or dynamical similarity) between the collective dynamics of the aligned proteins. The RMSIP allows the quantitative comparison of C_{α} atoms' fluctuations between proteins, and its values range from 0 to 1; an RMSIP of 1 represents maximum similarity in C_{α} atoms' fluctuations between compared proteins. WebNM@ also provides a graph of the C_{α} atoms fluctuations. Here, the normalized squared C_{α} atoms' fluctuations for each protein were calculated as the sum of the displacement of each C_{α} atom along with the lowest modes [32]. The fluctuations are the sum of the C_{α} atoms' displacements in each mode weighted by the inverse of their corresponding eigenvalues. The first 200 modes were used to carry out these calculations. Flexible protein regions can be inferred by inspecting the peaks in the fluctuations graph.

4.3. Cloning, Expression, and Purification

All chemicals and IMAC-Select Affinity Gel resin were purchased from Sigma-Aldrich (Milan, Italy); restriction enzymes and T4 DNA Ligase from New England Biolabs (Ipswich, MA, USA); Phusion™ High-fidelity DNA polymerase from Finnzymes (Espoo, Finland); TSAP (Thermosensitive Alkaline Phosphatase) from Promega (Milan, Italy). Ketone compounds for enzyme assays were dissolved in dioxane at 1 M concentration. A synthetic gene encoding *HtBVMO* was purchased by GeneArt®-Life Technologies (Regensburg, Germany), and cloned into a pMK-RQ plasmid, in between the sites NcoI/NotI, which were exploited for cloning in a pET-28a (+) vector. The recombinant enzyme *HtBVMO* was expressed in *E. coli* BL21 (DE3). Pre-cultured cells (at 37 °C in LB medium containing 50 µg/mL kanamycin) were grown in 800 mL of LB medium in a shaking incubator at 37 °C to $OD_{600} = 0.6$, then induced, by the addition of IPTG, to a final concentration of 0.2 mM

and cultivated at 12 °C for 60 h. Cells were harvested by centrifugation (4 °C, 10 min, 5000 g) and resuspended in 20 mL of 50 mM Tris-HCl buffer, pH 8.0. FAD was added to the cell suspension at 100 µM concentration before disruption by French Press. Twelve mL of 5.0 M NaCl in Tris/HCl buffer were slowly added to the cell lysate and the final solution (containing 2.0 M NaCl) was incubated at 4 °C overnight. Cellular debris were separated by centrifugation at 18,000 g for 30 min at 4 °C. The first step of purification was performed by immobilized-metal affinity chromatography (IMAC; BioRad, Milan, Italy). His-Select Nickel Affinity gel was placed in a Poly-Prep column (BioRad) by gravity flow and equilibrated with 50 mM Tris-HCl, 2.0 M NaCl, pH 8.0. The supernatant fraction of cell lysate was loaded onto the column, and washed by gravity flow with 50 mM Tris-HCl, 2.0 M NaCl. Elution was performed by the addition of five column volumes of 50 mM Tris/HCl, 2.0 M NaCl, 250 mM imidazole. The second step of purification was performed by hydrophobic chromatography. The imidazole elution was loaded (0.5 mL/min) on a butyl-sepharose column (HiScreen™ Butyl FF; GE Healthcare, Milan, Italy) pre-equilibrated with 50 mM TRIS-HCl, 2.0 M NaCl buffer. The protein was eluted by adding one column volume of the same equilibration buffer. The eluted fraction was concentrated by membrane filtration using a Vivaspin 6 Centrifugal Concentrator (30,000 mw cut-off) (Sartorius, Goettingen, Germany). Enzyme concentration was determined spectrophotometrically, by measuring the concentration of free flavin in a solution of denatured protein and calculated as previously reported [71].

4.4. In-Gel Digestion and Extraction of Peptides for ESI MS

The band corresponding to the recombinant protein was excised from the polyacrylamide gel, chopped into small pieces and washed with 150 µL water. Between three and four volumes of acetonitrile were added, and gel material was left to shrink at room temperature for about 15 min. Acetonitrile was then removed, and the gel material was dried. The gel pieces were then swelled in 10 mM TCEP/0.1 M NH₄HCO₃, incubated for 30 min at 56 °C and shrunk again in acetonitrile, then dried and incubated for 15 min in 55 mM iodoacetamide/0.1 M NH₄HCO₃. After shrinking and drying, the gel pieces were incubated in 50 mM NH₄HCO₃ and 12.5 ng/µL trypsin at 4 °C for 30 min and overnight at 37 °C. After overnight incubation, 50 µL of 5% formic acid was added to the digestion mix and incubated for 15 min at 37 °C. Two volumes of acetonitrile were added to the mix, which was centrifuged, and the supernatant, containing the digested peptides, was collected. Before injection in ESI MS, peptides were resuspended in 50% acetonitrile and 0.1% formic acid in water.

4.5. Enzymatic Activity Measurements and Kinetic Characterization

HtBVMO activity was spectrophotometrically determined by monitoring the decrease in NADPH at 340 nm ($\epsilon = 6.22 \text{ mM}^{-1}\text{cm}^{-1}$). Reaction mixtures (100 µL) contained 50 mM Tris-HCl buffer pH 8.0, 100 µM NADPH, 10 mM nonan-3-one and different salt concentrations. Reactions were started by adding the pure enzyme to the mixtures to a final concentration ranging 2–4 µM. One unit of BVMO is defined as the amount of protein that oxidizes 1 µmol NADPH per minute. The influence of salt concentration on HtBVMO activity was analyzed using different concentrations of NaCl (0–5.0 M) and KCl (0–4.0 M) and nonan-3-one as substrate. The effect of pH was studied over the 6–10 range using nonan-3-one as substrate and a fixed concentration of 2.0 M NaCl in 100 mM Tris, 50 mM MES, and 50 mM AcOH. Steady-state kinetic parameters of the different substrates were determined using substrate concentrations ranging from 0 to 20 mM and a concentration of 2.0 M NaCl in the reaction mixture. Data were fitted by the Michaelis–Menten equation using GraphPad Prism.

4.6. Circular Dichroism

The circular spectra of HtBVMO in 50 mM TRIS-HCl pH 8 in the presence of an increasing NaCl concentration were obtained by a Jasco J-710 instrument (Tokyo-Japan). The far-UV spectra were recorded using a 1 mm quartz cuvette and a protein concentration of 0.1 mg/mL; for the near-UV spectra, a 1 cm cuvette and a protein concentration of 0.5 mg/mL were used. The mean residue

ellipticity ϑ_{MRW} ($\text{deg cm}^2 \text{dmol}^{-1}$) was calculated by the formula $\vartheta_{MRW} = (\vartheta_{\text{obs}} \times MRW) / (10 \times l \times c)$, where “ ϑ_{obs} ” is the observed ellipticity signal, “ MRW ” is the mean residue molecular weight of the protein, “ l ” is the optical path length in cm and “ c ” is the protein concentration in g/mL. The k2d3 deconvolution method [72] was used to estimate the α -helical content [73].

4.7. ThermoFluor

Unfolding temperatures, T_{ms} , were determined by using the ThermoFluor® method. The purified enzyme at 5 μM concentration was added to 44 μL of the chosen buffer in a 96-well plate. 5 μL of Sypro-Orange, diluted 1:100 in H_2O , were mixed to each sample. The plate was loaded on a Real-Time PCR machine fitted with a 470–543 nm excitation filter and a SYBR Green emission filter (523–543 nm). A temperature gradient from 20 to 90 $^\circ\text{C}$ was applied (1 $^\circ\text{C}/\text{min}$), and fluorescence data were recorded. A sigmoidal curve was obtained after plotting the fluorescence against the temperature. T_{ms} were then determined as the maximum of the derivative of the sigmoidal curve.

4.8. Conversions and GC-MS Analysis

For GC-MS analysis, 5 mL of 50 mM Tris/HCl (pH 8.0), containing 1.0 M NaCl, 5 mM substrate, 100 μM NADPH, 34 μM PTDH, 20 mM phosphite and 34 μM *Ht*BVMO was incubated at 24 $^\circ\text{C}$ for 20 h. The reactions were carried out in glass vessels of 20 mL volumes closed with air-tight stoppers. The reactions were then stopped by heating for 20 min at 60 $^\circ\text{C}$ and analyzed by headspace GC-MS. 250 μL of the headspace of the vial was injected and analyzed in a GCMS-QP2010 (Shimadzu, Kyoto, Japan) equipped with an HP-1 column (30 m \times 0.25 mm \times 0.25 μm , Agilent, Santa Clara, CA, USA). Detection was carried out using 5 min hold at 35 $^\circ\text{C}$; heating ramp from 35 $^\circ\text{C}$ to 250 $^\circ\text{C}$ at a rate of 20 $^\circ\text{C}$ per minute; and 5 min hold at 250 $^\circ\text{C}$. Substrates to products transformation were determined based on the % peak area of product and substrate ketones.

4.9. Biotransformations and GC Analysis

Whole-cell biotransformations were performed using resting cells. Flasks with 25 mL of LB medium were inoculated with precultures of *E. coli* BL21 cells carrying the *Ht*BVMO- or the *Cm*BVMO-expression vector. Cells were grown at 37 $^\circ\text{C}$, 180 rpm, in a shaker incubator. After reaching an optical density of 0.6, IPTG and riboflavin were added to the culture at 0.2 mM and 20 μM concentrations, respectively. During the expression phase, cells were incubated for 48 h at 12 $^\circ\text{C}$ shaking at 180 rpm. Cells were harvested by centrifugation and resuspended in 5 mL of 100 mM sodium phosphate, pH 7.2, containing 5 mM substrate and 50 mM glucose; then, they were further incubated at 20 $^\circ\text{C}$ for 48 h at 200 rpm. The products of the biotransformations were extracted with 5 mL of ethyl acetate, concentrated by a rotatory evaporator and resuspended to a final volume of 0.5 mL ethyl acetate. Samples were analyzed using a GC-2010 gas chromatograph (Shimadzu, Kyoto, Japan) equipped with 60 m \times 0.53 mm \times 1 μm INNOVAX column. The detection of products from nonan-3-one bioconversion was carried out using the following temperature program: hold 10 min at 75 $^\circ\text{C}$; heating ramp from 75 to 240 $^\circ\text{C}$ at a rate of 50 $^\circ\text{C}$ per minute; hold 2 min at 240 $^\circ\text{C}$. The detection of products from heptan-2-one bioconversion was carried out using: hold 10 min at 70 $^\circ\text{C}$; heating ramp from 70 to 240 $^\circ\text{C}$ at a rate of 50 $^\circ\text{C}$ per minute; hold 2 min at 240 $^\circ\text{C}$. The injector and detector temperature were maintained at 270 $^\circ\text{C}$.

Supplementary Materials: The following are available online at <http://www.mdpi.com/2073-4344/10/1/128/s1>; Figure S1: Multiple sequence alignment, Figure S2: WEBPIPSA heatmap of the electrostatic distance (ED) among BVMOs, Figure S3: WEBPIPSA epogram of BVMOs, Figure S4: Class 1 (a) and Class 5 (b) heat map of BC showing the dynamic relatedness between proteins, Figure S5: SDS-PAGE analysis of total cell extracts from *E. coli* and purified *Ht*BVMO protein, Figure S6: GC analysis of products from whole cell biotransformations, Table S1: Comparison of BVMO net charge, Table S2: BVMO dataset used for comparative electrostatics analyses.

Author Contributions: M.N. and E.B. (Elisa Beneventi) conceived and designed the study. I.R. and F.F. performed structural modeling, electrostatics analysis and NMA. M.N. carried out the experimental investigations, to which E.B. (Elisa Beneventi) initially contributed. P.P.d.L. and M.W.F. collaborated to the work, providing skills and

facilities. M.N. and I.R. prepared the first draft of the manuscript, F.F. and E.B. (Elisabetta Bergantino) wrote, reviewed and edited its final form. All authors have read and agreed to the published version of the manuscript.

Funding: This research was funded by F.I.S.-Fabbrica Italiana Sintetici (Alte di Montecchio Maggiore, Italy) and by the *Assegno di Ricerca* CPDR 159713/15 from the University of Padova entitled “Studying enzymes from extremophiles as tools for biocatalysis”.

Acknowledgments: We thank L. Cendron (Department of Biology, University of Padova, Italy) and Paolo Centomo (Department of Chemical Sciences, University of Padova, Italy) for helping in the *ThermoFluor* analysis of the recombinant *HtBVMO* and in the GC-MS analysis of whole-cell transformations, respectively.

Conflicts of Interest: The authors declare no conflict of interest. The funders had no role in the design of the study; in the collection, analyses, or interpretation of data; in the writing of the manuscript, or in the decision to publish the results.

References

1. Krow, G.R. The Baeyer–Villiger oxidation of ketones and aldehydes. *Org. React.* **2004**, *43*, 251–798.
2. Ten Brink, G.-J.; Arends, I.; Sheldon, R.A. The Baeyer–Villiger reaction: New developments toward greener procedures. *Chem. Rev.* **2004**, *104*, 4105–4124. [[CrossRef](#)]
3. Kamerbeek, N.M.; Olsthoorn, A.J.; Fraaije, M.W.; Janssen, D.B. Substrate specificity and enantioselectivity of 4-hydroxyacetophenone monooxygenase. *Appl. Environ. Microbiol.* **2003**, *69*, 419–426. [[CrossRef](#)] [[PubMed](#)]
4. Sarmiento, F.; Peralta, R.; Blamey, J.M. Cold and Hot Extremozymes: Industrial Relevance and Current Trends. *Front. Bioeng. Biotechnol.* **2015**, *3*, 148. [[CrossRef](#)] [[PubMed](#)]
5. Malito, E.; Alfieri, A.; Fraaije, M.W.; Mattevi, A. Crystal structure of a Baeyer–Villiger monooxygenase. *Proc. Natl. Acad. Sci. USA* **2004**, *101*, 13157–13162. [[CrossRef](#)] [[PubMed](#)]
6. Romero, E.; Castellanos, J.; Mattevi, A.; Fraaije, M.W. Characterization and Crystal Structure of a Robust Cyclohexanone Monooxygenase. *Angew. Chem. Int. Ed.* **2016**, *55*, 15852–15855. [[CrossRef](#)] [[PubMed](#)]
7. Fürst, M.J.L.J.; Savino, S.; Dudek, H.M.; Gómez Castellanos, J.R.; Gutiérrez de Souza, C.; Rovida, S.; Fraaije, M.W.; Mattevi, A. Polycyclic Ketone Monooxygenase from the Thermophilic Fungus *Thermothelomyces thermophila*: A Structurally Distinct Biocatalyst for Bulky Substrates. *J. Am. Chem. Soc.* **2017**, *139*, 627–630. [[CrossRef](#)] [[PubMed](#)]
8. Saunders, E.; Tindall, B.J.; Fähnrich, R.; Lapidus, A.; Copeland, A.; Del Rio, T.G.; Lucas, S.; Chen, F.; Tice, H.; Cheng, J.F.; et al. Complete genome sequence of *Haloterrigena turkmenica* type strain (4k T). *Stand. Genom. Sci.* **2010**, *2*, 107. [[CrossRef](#)] [[PubMed](#)]
9. Van Den Burg, B. Extremophiles as a source for novel enzymes. *Curr. Opin. Microbiol.* **2003**, *6*, 213–218. [[CrossRef](#)]
10. Elleuche, S.; Schröder, C.; Sahm, K.; Antranikian, G. Extremozymes—Biocatalysts with unique properties from extremophilic microorganisms. *Curr. Opin. Biotechnol.* **2014**, *29*, 116–123. [[CrossRef](#)]
11. Amoozgar, M.A.; Siroosi, M.; Atashgahi, S.; Smidt, H.; Ventosa, A. Systematics of haloarchaea and biotechnological potential of their hydrolytic enzymes. *Microbiology* **2017**, *163*, 623–645. [[CrossRef](#)]
12. Singh, A.; Singh, A.K. Haloarchaea: Worth exploring for their biotechnological potential. *Biotechnol. Lett.* **2017**, *39*, 1793–1800. [[CrossRef](#)] [[PubMed](#)]
13. Sellek, G.A.; Chaudhuri, J.B. Biocatalysis in organic media using enzymes from extremophiles. *Enzym. Microb. Technol.* **1999**, *25*, 471–482. [[CrossRef](#)]
14. Manikandan, K.; Bhardwaj, A.; Gupta, N.; Lokanath, N.K.; Ghosh, A.; Reddy, V.S.; Ramakumar, S. Crystal structures of native and xylosaccharide-bound alkali thermostable xylanase from an alkalophilic *Bacillus* sp. NG-27: Structural insights into alkalophilicity and implications for adaptation to polyextreme conditions. *Protein Sci.* **2006**, *15*, 1951–1960. [[CrossRef](#)] [[PubMed](#)]
15. Fraaije, M.W.; Kamerbeek, N.M.; van Berkel, W.J.H.; Janssen, D.B. Identification of a Baeyer–Villiger monooxygenase sequence motif. *FEBS Lett.* **2002**, *518*, 43–47. [[CrossRef](#)]
16. Vallon, O. New sequence motifs in flavoproteins: Evidence for common ancestry and tools to predict structure. *Proteins* **2000**, *38*, 95–114. [[CrossRef](#)]
17. Riebel, A.; Dudek, H.M.; de Gonzalo, G.; Stepniak, P.; Rychlewski, L.; Fraaije, M.W. Expanding the set of rhodococcal Baeyer–Villiger monooxygenases by high-throughput cloning, expression and substrate screening. *Appl. Microbiol. Biotechnol.* **2012**, *95*, 1479–1489. [[CrossRef](#)]

18. Beier, A.; Bordewick, S.; Genz, M.; Schmidt, S.; van den Bergh, T.; Peters, C.; Joosten, H.J.; Bornscheuer, U.T. Switch in Cofactor Specificity of a Baeyer-Villiger Monooxygenase. *Chembiochem* **2016**, *17*, 2312–2315. [[CrossRef](#)]
19. Bordoli, L.; Kiefer, F.; Arnold, K.; Benkert, P.; Battey, J.; Schwede, T. Protein structure homology modeling using SWISS-MODEL workspace. *Nat. Protoc.* **2009**, *4*, 1–13. [[CrossRef](#)]
20. Wang, Q.; Canutescu, A.A.; Dunbrack, R.L., Jr. SCWRL and MolIDE: Computer programs for side-chain conformation prediction and homology modeling. *Nat. Protoc.* **2008**, *3*, 1832–1847. [[CrossRef](#)]
21. Benkert, P.; Kunzli, M.; Schwede, T. QMEAN server for protein model quality estimation. *Nucleic Acids Res.* **2009**, *37*, W510–W514. [[CrossRef](#)] [[PubMed](#)]
22. Britton, K.L.; Baker, P.J.; Fisher, M.; Ruzheinikov, S.; Gilmour, D.J.; Bonete, M.J.; Ferrer, J.; Pire, C.; Esclapez, J.; Rice, D.W. Analysis of protein solvent interactions in glucose dehydrogenase from the extreme halophile *Haloferax mediterranei*. *Proc. Natl. Acad. Sci. USA* **2006**, *103*, 4846–4851. [[CrossRef](#)] [[PubMed](#)]
23. Dym, O.; Mevarech, M.; Sussman, J.L. Structural features that stabilize halophilic malate dehydrogenase from an archaeobacterium. *Science* **1995**, *267*, 1344–1346. [[CrossRef](#)] [[PubMed](#)]
24. Frolow, F.; Harel, M.; Sussman, J.L.; Mevarech, M.; Shoham, M. Insights into protein adaptation to a saturated salt environment from the crystal structure of a halophilic 2Fe-2S ferredoxin. *Nat. Struct. Mol. Biol.* **1996**, *3*, 452–458. [[CrossRef](#)]
25. Paul, S.; Bag, S.K.; Das, S.; Harvill, E.T.; Dutta, C. Molecular signature of hypersaline adaptation: Insights from genome and proteome composition of halophilic prokaryotes. *Genome Biol.* **2008**, *9*, R70. [[CrossRef](#)]
26. Tadeo, X.; López-Méndez, B.; Trigueros, T.; Laín, A.; Castaño, D.; Millet, O. Structural basis for the aminoacid composition of proteins from halophilic archaea. *PLoS Biol.* **2009**, *7*, e1000257. [[CrossRef](#)]
27. Chakravorty, D.; Khan, M.F.; Patra, S. Multifactorial level of extremostability of proteins: Can they be exploited for protein engineering? *Extremophiles* **2017**, *21*, 419–444. [[CrossRef](#)]
28. Ceccoli, R.D.; Bianchi, D.A.; Fink, M.J.; Mihovilovic, M.D.; Rial, D.V. Cloning and characterization of the Type I Baeyer-Villiger Monooxygenase from *Leptospira biflexa*. *AMB Express* **2017**, *7*, 87. [[CrossRef](#)]
29. Righetto, I.; Milani, A.; Cattoli, G.; Filippini, F. Comparative structural analysis of haemagglutinin proteins from type A influenza viruses: Conserved and variable features. *BMC Bioinform.* **2014**, *15*, 363. [[CrossRef](#)]
30. Heidari, A.; Righetto, I.; Filippini, F. Electrostatic Variation of Haemagglutinin as a Hallmark of the Evolution of Avian Influenza Viruses. *Sci. Rep.* **2018**, *8*, 1929. [[CrossRef](#)]
31. Meeuwssen, S.M.; Hodac, A.N.; Adams, L.M.; McMunn, R.D.; Anschutz, M.S.; Carothers, K.J.; Egdorf, R.E.; Hanneman, P.M.; Kitzrow, J.P.; Keonigsberg, C.K.; et al. Investigation of intrinsic dynamics of enzymes involved in metabolic pathways using coarse-grained normal mode analysis. *Cogent Biol.* **2017**, *3*, 1. [[CrossRef](#)]
32. Tiwari, S.P.; Fuglebakk, E.; Hollup, S.M.; Skjærven, L.; Cragolini, T.; Grindhaug, S.H.; Tekle, K.M.; Reuter, N. WEBnm@ v2.0: Web server and services for comparing protein flexibility. *BMC Bioinform.* **2014**, *15*, 427. [[CrossRef](#)] [[PubMed](#)]
33. Martin, D.D.; Ciulla, R.A.; Roberts, M.F. Osmoadaptation in archaea. *Appl. Environ. Microbiol.* **1999**, *65*, 1815–1825. [[CrossRef](#)] [[PubMed](#)]
34. Madern, D.; Zaccari, G. Molecular adaptation: The malate dehydrogenase from the extreme halophilic bacterium *Salinibacter ruber* behaves like a non-halophilic protein. *Biochimie* **2004**, *86*, 295–303. [[CrossRef](#)] [[PubMed](#)]
35. Eddy, M.L.; Jablonski, P.E. Purification and characterization of a membrane-associated ATPase from *Natronococcus occultus*, a haloalkaliphilic archaeon. *FEMS Microbiol. Lett.* **2000**, *189*, 211–214. [[CrossRef](#)] [[PubMed](#)]
36. Müller-Santos, M.; de Souza, E.M.; Pedrosa, F.O.; Mitchell, D.A.; Longhi, S.; Carrière, F.; Canaan, S.; Krieger, N. First evidence for the salt-dependent folding and activity of an esterase from the halophilic archaeon *Haloarcula marismortui*. *Biochim. Biophys. Acta* **2009**, *1791*, 719–729. [[CrossRef](#)]
37. Ellis, K.J.; Morrison, J.F. Buffers of constant ionic strength for studying pH-dependent processes. *Methods Enzymol.* **1982**, *87*, 405–426. [[CrossRef](#)]
38. Kelly, S.M.; Jess, T.J.; Price, N.C. How to study proteins by circular dichroism. *Biochim. Biophys. Acta* **2005**, *1751*, 119–139. [[CrossRef](#)]
39. Costas, A.M.; White, A.K.; Metcalf, W.W. Purification and characterization of a novel phosphorus-oxidizing enzyme from *Pseudomonas stutzeri* WM88. *J. Biol. Chem.* **2001**, *276*, 17429–17436. [[CrossRef](#)]

40. Ebel, C.; Faou, P.; Kernel, B.; Zaccai, G. Relative role of anions and cations in the stabilization of halophilic malate dehydrogenase. *Biochemistry* **1999**, *38*, 9039–9047. [[CrossRef](#)]
41. Beneventi, E.; Niero, M.; Motterle, R.; Fraaije, M.; Bergantino, E. Discovery of Baeyer-Villiger monooxygenases from photosynthetic eukaryotes. *J. Mol. Catal. B Enzym.* **2013**, *98*, 145–154. [[CrossRef](#)]
42. Zaccai, G.; Eisenberg, H. Halophilic proteins and the influence of solvent on protein stabilization. *Trends Biochem. Sci.* **1990**, *15*, 333–337. [[CrossRef](#)]
43. Castle, A.M.; Macnab, R.M.; Shulman, R.G. Measurement of intracellular sodium concentration and sodium transport in *Escherichia coli* by ²³Na nuclear magnetic resonance. *J. Biol. Chem.* **1986**, *261*, 3288–3294. [[PubMed](#)]
44. Bonete, M.-J.; Pire, C.; Llorca, F.I.; Camacho, M.L. Glucose dehydrogenase from the halophilic Archaeon *Haloferax mediterranei*: Enzyme purification, characterisation and N-terminal sequence. *FEBS Lett.* **1996**, *383*, 227–229. [[CrossRef](#)]
45. Torres, S.; Castro, G.R. Non-aqueous biocatalysis in homogeneous solvent systems. *Food Technol. Biotechnol.* **2004**, *42*, 271–277.
46. Ruiz, D.M.; De Castro, R.E. Effect of organic solvents on the activity and stability of an extracellular protease secreted by the haloalkaliphilic archaeon *Natrialba magadii*. *J. Ind. Microbiol. Biotechnol.* **2007**, *34*, 111–115. [[CrossRef](#)]
47. Elbanna, K.; Ibrahim, I.M.; Revol-Junelles, A.-M. Purification and characterization of halo-alkali-thermophilic protease from Halobacterium. *Extremophiles* **2015**, *19*, 763–774. [[CrossRef](#)]
48. Munawar, N.; Engel, P.C. Overexpression in a non-native halophilic host and biotechnological potential of NAD-dependent glutamate dehydrogenase from *Halobacterium salinarum* strain NRC-36014. *Extremophiles* **2012**, *16*, 463–476. [[CrossRef](#)]
49. Alsafadi, D.; Paradisi, F. Effect of organic solvents on the activity and stability of halophilic alcohol dehydrogenase (ADH2) from *Haloferax volcanii*. *Extremophiles* **2013**, *17*, 115–122. [[CrossRef](#)]
50. Fukushima, T.; Mizuki, T.; Echigo, A.; Inoue, A.; Usami, R. Organic solvent tolerance of halophilic α -amylase from a Haloarchaeon, *Haloarcula* sp. strain S-1. *Extremophiles* **2005**, *9*, 85–89. [[CrossRef](#)]
51. Chang, J.; Lee, Y.-S.; Fang, S.-J. Recombinant expression and characterization of an organic-solvent-tolerant α -amylase from *Exiguobacterium* sp. DAU5. *Appl. Biochem. Biotechnol.* **2013**, *169*, 1870–1883. [[CrossRef](#)] [[PubMed](#)]
52. Opperman, D.J.; Reetz, M.T. Towards Practical Baeyer–Villiger-Monooxygenases: Design of Cyclohexanone Monooxygenase Mutants with Enhanced Oxidative Stability. *ChemBiochem* **2010**, *11*, 2589–2596. [[CrossRef](#)] [[PubMed](#)]
53. Van Beek, H.L.; Wijma, H.J.; Fromont, L.; Janssen, D.B.; Fraaije, M.W. Stabilization of cyclohexanone monooxygenase by a computationally designed disulfide bond spanning only one residue. *FEBS Open Biol.* **2014**, *4*, 168–174. [[CrossRef](#)] [[PubMed](#)]
54. Schmidt, S.; Genz, M.; Balke, K.; Bornscheuer, U.T. The effect of disulfide bond introduction and related Cys/Ser mutations on the stability of a cyclohexanone monooxygenase. *J. Biotechnol.* **2015**, *214*, 199–211. [[CrossRef](#)] [[PubMed](#)]
55. Sievers, F.; Wilm, A.; Dineen, D.; Gibson, T.J.; Karplus, K.; Li, W.; Lopez, R.; McWilliam, H.; Remmert, M.; Söding, J.; et al. Fast, scalable generation of high-quality protein multiple sequence alignments using Clustal Omega. *Mol. Syst. Biol.* **2011**, *7*, 539. [[CrossRef](#)] [[PubMed](#)]
56. *E. coli* Codon Usage Analyzer 2.1. Available online: <http://www.faculty.ucr.edu> (accessed on 11 December 2019).
57. Wilkins, M.R.; Gasteiger, E.; Bairoch, A.; Sanchez, J.C.; Williams, K.L.; Appel, R.D.; Hochstrasser, D.F. Protein identification and analysis tools on the ExPASy server. *Methods Mol. Biol.* **1999**, *112*, 531–552. [[CrossRef](#)]
58. Biasini, M.; Bienert, S.; Waterhouse, A.; Arnold, K.; Studer, G.; Schmidt, T.; Kiefer, F.; Gallo Cassarino, T.; Bertoni, M.; Bordoli, L.; et al. SWISS-MODEL: Modelling protein tertiary and quaternary structure using evolutionary information. *Nucleic Acids Res.* **2014**, *42*, W252–W258. [[CrossRef](#)]
59. Pettersen, E.F.; Goddard, T.D.; Huang, C.C.; Couch, G.S.; Greenblatt, D.M.; Meng, E.C.; Ferrin, T.E. UCSF Chimera—A visualization system for exploratory research and analysis. *J. Comput. Chem.* **2004**, *25*, 1605–1612. [[CrossRef](#)]
60. UCSF Chimera. Available online: <http://www.cgl.ucsf.edu/chimera/> (accessed on 11 December 2019).

61. Dolinsky, T.J.; Czodrowski, P.; Li, H.; Nielsen, J.E.; Jensen, J.H.; Klebe, G.; Baker, N.A. PDB2PQR: Expanding and upgrading automated preparation of biomolecular structures for molecular simulations. *Nucleic Acids Res.* **2007**, *35*, W522–W525. [[CrossRef](#)]
62. Sitkoff, D.; Sharp, K.A.; Honig, B. Accurate calculation of hydration free energies using macroscopic solvent models. *J. Phys. Chem.* **1994**, *98*, 1978–1988. [[CrossRef](#)]
63. Baker, N.A.; Sept, D.; Joseph, S.; Holst, M.J.; McCammon, J.A. Electrostatics of nanosystems: Application to microtubules and the ribosome. *Proc. Natl. Acad. Sci. USA* **2001**, *98*, 10037–10041. [[CrossRef](#)]
64. Opal Web Service. Available online: <http://www.poissonboltzmann.org/apbs> (accessed on 11 December 2019).
65. Schutz, C.N.; Warshel, A. What are the dielectric “constants” of proteins and how to validate electrostatic models? *Proteins* **2001**, *44*, 400–417. [[CrossRef](#)] [[PubMed](#)]
66. Gorham, R.D., Jr.; Kieslich, C.A.; Morikis, D. Electrostatic clustering and free energy calculations provide a foundation for protein design and optimization. *Ann. Biomed. Eng.* **2011**, *39*, 1252–1263. [[CrossRef](#)] [[PubMed](#)]
67. Lee, K.K.; Fitch, C.A.; Garcia-Moreno, E.B. Distance dependence and salt sensitivity of pairwise, coulombic interactions in a protein. *Protein Sci.* **2002**, *11*, 1004–1016. [[CrossRef](#)] [[PubMed](#)]
68. WebPIPSA Server. Available online: <http://pipsa.eml.org/pipsa> (accessed on 11 December 2019).
69. Fraczekiewicz, R.; Braun, W. Exact and efficient analytical calculation of the accessible surface areas and their gradients for macromolecules. *J. Comput. Chem.* **1998**, *19*, 319–333. [[CrossRef](#)]
70. Krissinel, E. On the relationship between sequence and structure similarities in proteomics. *Bioinformatics* **2007**, *23*, 717–723. [[CrossRef](#)] [[PubMed](#)]
71. Fraaije, M.W.; Wu, J.; Heuts, D.P.H.M.; van Hellemond, E.W.; Spelberg, J.H.; Janssen, D.B. Discovery of a thermostable Baeyer–Villiger monooxygenase by genome mining. *Appl. Microbiol. Biotechnol.* **2005**, *66*, 393–400. [[CrossRef](#)]
72. K2D3. Available online: <http://cbdm-01.zdv.uni-mainz.de/~{andrade/k2d3/> (accessed on 11 December 2019).
73. Louis-Jeune, C.; Andrade-Navarro, M.A.; Perez-Iratxeta, C. Prediction of protein secondary structure from circular dichroism using theoretically derived spectra. *Proteins* **2012**, *80*, 374–381. [[CrossRef](#)]



© 2020 by the authors. Licensee MDPI, Basel, Switzerland. This article is an open access article distributed under the terms and conditions of the Creative Commons Attribution (CC BY) license (<http://creativecommons.org/licenses/by/4.0/>).